Transport in Porous Media (2006) 64: 339–373
DOI 10.1007/s11242-005-5049-z

Analytical Solutions to Multiphase First-Contact Miscible Models with Viscous Fingering

RUBEN JUANES[1,*] and MARTIN J. BLUNT[2]
[1]*Department of Petroleum Engineering, Stanford University, 65 Green Earth Sciences Bldg., Stanford, CA 94305, USA*
[2]*Department of Earth Science and Engineering, Imperial College, London SW7 2AZ, UK*

(Received 8 March 2005; accepted in final form: 2 November 2005)

Abstract. In this paper, we analyze an empirical model of viscous fingering for three-component, two-phase, first-contact miscible flows. We present the complete range of analytical solutions to secondary and tertiary water-alternating-gas (WAG) floods. An important ingredient in the construction of analytical solutions is the presence of detached (nonlocal) branches of the Hugoniot locus, that is, curves in composition space that satisfy the Rankine–Hugoniot conditions but do not contain the reference state. We illustrate how, in water–solvent floods into a medium with mobile water and residual oil (immobile to water), the solvent front and the water Buckley–Leverett front may interact, resulting in a leading water/solvent shock that is stable to viscous fingering. The analytical solutions explain why in these miscible tertiary floods, oil and solvent often break through simultaneously. We discuss the implications of the new solutions in the design of miscible tertiary floods, such as the estimation of the optimum WAG ratio.

Key words: miscible flooding, viscous fingering, water-alternating-gas, optimum WAG ratio, Riemann problem, Hugoniot locus, detached branches.

1. Introduction

Solvent injection is a commonly used technology for enhanced oil recovery in hydrocarbon reservoirs (Stalkup, 1983; Lake, 1989), and it can be a viable option for environmental remediation of groundwater pollution by nonaqueous phase liquids (Khan *et al.*, 1996). The objective of solvent flooding is to develop miscibility between the resident and injected hydrocarbon phases, thereby mobilizing the residual oil, and enhancing the mobility of the hydrocarbon phase. One of the key technical and practical aspects of miscible flooding is the development of fluid instabilities in

*Author for correspondence. Now at the Department of Petroleum and Geosystems Engineering, The University of Texas, Austin, Texas 78712, USA. e-mail: juanes@mail.utexas.edu

the form of viscous fingering when a low viscosity fluid (solvent) is injected into a formation filled with more viscous fluids (water and oil) (Saffman and Taylor, 1958).

Despite its high local displacement efficiency, the overall effectiveness of solvent injection may be compromised by the low sweep efficiency associated with an unstable displacement process: the solvent fingers through the porous medium, leading to early breakthrough and leaving much of the oil behind. Simultaneous injection of solvent and water has shown to be effective at limiting the degree of fingering, by reducing the mobility contrast between the injected and displaced fluids (Caudle and Dyes, 1958). In practice, water and solvent are injected in alternating slugs in a process called water-alternating-gas or WAG. Thus, we shall refer to WAG injection even though, strictly speaking, we mean simultaneous water–solvent injection.

Viscous fingering in porous media flows has been studied at length over the past few decades. A comprehensive review of this phenomenon is given by Homsy (1987). Viscous fingering can only occur in a multidimensional scenario that allows for interface instabilities to develop. There are two modeling approaches: (1) high-resolution numerical simulations that capture the details of the viscous fingering phenomenon (Christie and Jones, 1987; Tan and Homsy, 1988; Christie, 1989; Zimmerman and Homsy, 1991; Christie *et al.*, 1993; Tchelepi and Orr, 1994; Chen Meiburg, 1998; Ruith and Meiburg, 2000) and (2) macroscopic models that capture just the relevant averaged behavior of these displacements such as breakthrough time and amounts of displaced and displacing fluids produced over time. In this investigation we concentrate on the latter approach.

While there is conclusive theoretical, computational and experimental evidence of the importance of viscous fingering in miscible displacements at adverse mobility ratios in homogeneous porous media, other factors such as permeability heterogeneity and gravity segregation may affect the displacement patterns in the field. Several investigations (Fayers *et al.*, 1992; Chang *et al.*, 1994; Tchelepi and Orr, 1994) suggest rather convincingly that if the permeability field is highly heterogeneous with large correlation lengths, the displacement will also be dominated by channeling of the injected solvent through the high-permeability streaks. Gravity override may also play a major role in three-dimensional displacements, especially in combination with large-scale heterogeneities (Christie *et al.*, 1990; Christie *et al.*, 1993; Chang *et al.*, 1994; Tchelepi and Orr, 1994).

In this investigation, we examine a rather simplified setting in which the medium is quasi-homogeneous and gravity forces are negligible. These conditions are such that viscous fingering is the dominant mechanism for pattern formation and, admittedly, may not be representative of the conditions often encountered in heterogeneous reservoirs. However, the study of viscous fingering under these assumptions is still of major interest:

(1) short correlation-length heterogeneity and moderate gravity effects can be included in macroscopic models of viscous fingering (Koval, 1963; Fayers *et al.*, 1992) and (2) conventional reservoir models do not capture the fine-scale heterogeneity of the medium and the details of the displacement patterns. Macroscopic models of viscous fingering are therefore useful as a means of accounting for viscous fingering within each simulation grid block (Todd and Longstaff, 1972; Christie *et al.*, 1993).

Empirical models of viscous fingering have been successful at predicting average behavior of unstable miscible floods of a single hydrocarbon phase (Koval, 1963; Todd and Longstaff, 1972). Such empirical models have later been extended and validated for three-component flows in which two of the components (solvent and oil) are completely miscible (Blunt and Christie, 1993, 1994), and for near-miscible compositional displacements (Blunt *et al.*, 1994).

In this paper, we revisit the analytical theory of first-contact miscible displacements in the presence of viscous fingering. We consider three-component flows (water, oil and solvent), and assume that oil and solvent mix in all proportions to form a single hydrocarbon phase, which is immiscible with the aqueous phase.

We employ the empirical model proposed by Blunt and Christie (1993, 1994). They used an extension of the Todd and Longstaff model (1972) to describe fingering of the solvent in a two-phase, three-component system. They proposed a self-consistency condition to calibrate the only parameter of the fingering model – the effective mobility ratio M_{eff}. Analytical solutions were obtained for secondary floods (water–solvent injection into a medium filled with mobile oil and immobile water) and tertiary floods (water–solvent injection into a medium filled with mobile water and immobile oil). They obtained an excellent agreement between analytical predictions using the empirical one-dimensional model and averaged saturation and concentration profiles from two-dimensional direct numerical simulations. Their analysis was restricted, however, to secondary and tertiary WAG floods in which the leading edge of the solvent front is slower than the water shock.

In this paper we provide a comprehensive analysis of the system of equations, and develop analytical solutions for secondary and tertiary floods in which no *a priori* assumption is made on the velocity of the solvent front. An important ingredient in the construction of analytical solutions is the presence of detached (nonlocal) branches of the Hugoniot locus, that is, curves in composition space that satisfy the Rankine–Hugoniot conditions but do not contain the reference state. We show that the analytical solution may comprise a leading water/solvent shock that is stable to viscous fingering. The analytical solutions explain why, in miscible tertiary floods, oil and solvent often break through

simultaneously. We anticipate that this result has important implications in the design of miscible tertiary floods.

The paper is organized as follows. In Section 2 we present the mathematical model, which leads to a system of two first-order partial differential equations. The character of the system of equations is analyzed in Section 3. In Section 4 we describe the complete catalogue of analytical solutions to the Riemann problem for secondary and tertiary floods, for any water–solvent injection ratio. In Section 5 we discuss further some of the relevant findings, and we illustrate how the results carry over to a model in which the effective mobility ratio is adapted dynamically. We specifically address the influence of viscous fingering on the estimation of the optimum water–solvent ratio. Finally we give some conclusions and recommendations in Section 6.

2. Mathematical Model

We study three-component (water, oil and solvent) flow in porous media under the following assumptions (Blunt and Christie, 1993):

1. Water forms an aqueous phase, which is immiscible with the two hydrocarbon components.
2. Oil and solvent mix in all proportions to form a single hydrocarbon phase.
3. All fluids are incompressible.
4. There is no volume change in mixing.
5. The medium is rigid.
6. The effects of gravity and capillarity are negligible.
7. We use a multiphase extension of Darcy's law (Muskat, 1949), with non-hysteretic relative permeabilities.

It is useful to discuss further some of these assumptions. We are interested in the limit of negligible capillarity. Such approximation is sensible when studying the large-scale behavior of viscous fingering in miscible systems. If the system is dominated by capillary forces, the instability in the fluid displacement is of an entirely different nature (capillary fingering), and neglecting capillary pressure between phases would not be appropriate (Lenormand *et al.*, 1988).

Hysteresis is not included in our analysis, that is, the relative permeability functions do not reflect history dependence. This means that trapping of the hydrocarbon phase *during* the water–solvent injection process is ignored. For pure solvent floods, this assumption is not a limiting one: the saturation of the (less wetting) hydrocarbon phase increases continuously, with the solvent forming a continuous advancing cluster, thereby precluding trapping. However, this effect may become significant in simultaneous

water–solvent injection, especially for secondary floods in which the water front moves faster than the solvent front: the injected water may disconnect some of the oil phase, making it less accessible for the solvent that travels at a lower velocity. In such cases, modeling of the trapped hydrocarbon phase may be necessary (Lin and Huang, 1990; O'Steen and Huang, 1990). The effects of hysteresis (responsible for trapping of the oil) may be even more relevant in water-alternating-gas applications (Spiteri and Juanes, 2006; Spiteri *et al.*, 2005).

Under the assumptions listed above, and ignoring the effect of viscous fingering, the one-dimensional model describing the problem is given by the following system of conservation equations (Juanes and Lie, 2005):

$$\frac{\partial S}{\partial t}+\frac{\partial f}{\partial x}=0, \tag{1}$$

$$\frac{\partial C}{\partial t}+\frac{\partial}{\partial x}\left((1-f)\frac{C}{1-S}\right)=0, \tag{2}$$

where x and t are dimensionless space and time variables, respectively, S is the water saturation, C is the solvent concentration, and f is the water fractional flow function. The solvent concentration is the overall volume fraction of solvent per unit pore volume:

$$C=(1-S)\chi, \tag{3}$$

where χ is the mass fraction of solvent in the hydrocarbon phase. The water fractional flow f is the velocity of the aqueous phase divided by the sum of the velocities of all flowing phases. When gravity and capillarity are neglected, it takes the following simple form:

$$f=\frac{\lambda_w}{\lambda_T}, \tag{4}$$

where $\lambda_T=\lambda_w+\lambda_h$ is the total mobility, and λ_α is the mobility of the α-phase, defined as

$$\lambda_\alpha=\frac{k_{r\alpha}}{\mu_\alpha}, \tag{5}$$

where $k_{r\alpha}$ is the relative permeability and μ_α is the dynamic viscosity of the α-phase. The viscosity of the hydrocarbon phase depends on the viscosities of the oil and solvent components μ_o and μ_s (taken as constants) and the mass fraction χ of solvent in the hydrocarbon phase. A common model for the hydrocarbon viscosity is the quarter-power rule (Koval, 1963; Todd and Longstaff, 1972):

$$\mu_h=\left[\frac{1-\chi}{\mu_o^{1/4}}+\frac{\chi}{\mu_s^{1/4}}\right]^{-4}. \tag{6}$$

Since the solvent viscosity is lower (usually much lower) than the oil viscosity, the hydrocarbon viscosity is a decreasing function of the solvent mass fraction. In Figure 1 we plot the hydrocarbon viscosity as a function of the solvent mass fraction for an oil–solvent viscosity ratio $M := \mu_o/\mu_s = 10$. In all the examples, we have used the following values of the fluid viscosities: $\mu_w = 1$ cp, $\mu_o = 4$ cp, and $\mu_s = 0.4$ cp.

We assume that the relative permeabilities are unique functions of the water saturation alone, therefore neglecting hysteresis effects and any dependence of the hydrocarbon residual saturation on the solvent content. In our examples, we have chosen a simple model with quadratic relative permeabilities (Figure 2):

$$k_{rw}(S) = \begin{cases} 0 & \text{if } S < S_{wc} = 0.2, \\ \left(\dfrac{S - S_{wc}}{1 - S_{wc}}\right)^2 & \text{otherwise,} \end{cases} \tag{7}$$

$$k_{rh}(S) = \begin{cases} 0 \quad \text{if } 1 - S < S_{hc} = 0.2, \\ 0.1\left(\dfrac{1 - S - S_{hc}}{1 - S_{hc}}\right) + 0.9\left(\dfrac{1 - S - S_{hc}}{1 - S_{hc}}\right)^2 \quad \text{otherwise.} \end{cases} \tag{8}$$

As a result, the fractional flow is a function of both water saturation and solvent concentration:

$$f = \frac{\frac{k_{rw}(S)}{\mu_w}}{\frac{k_{rw}(S)}{\mu_w} + \frac{k_{rh}(S)}{\mu_o\left((1-\chi) + M^{1/4}\chi\right)}} = f(S, C). \tag{9}$$

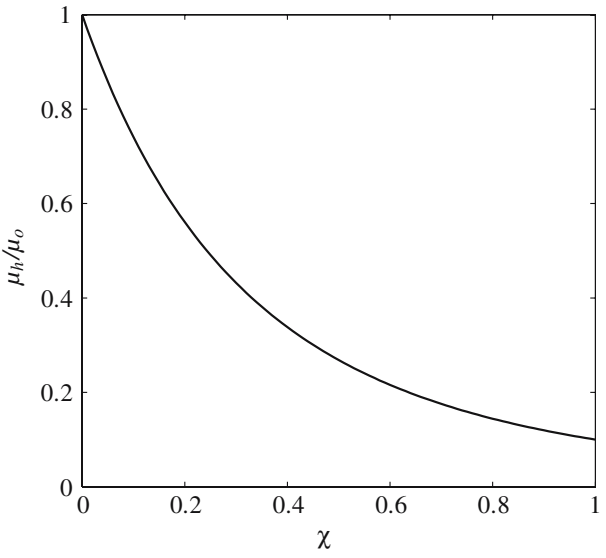

Figure 1. Dependence of the hydrocarbon viscosity on the solvent mass fraction.

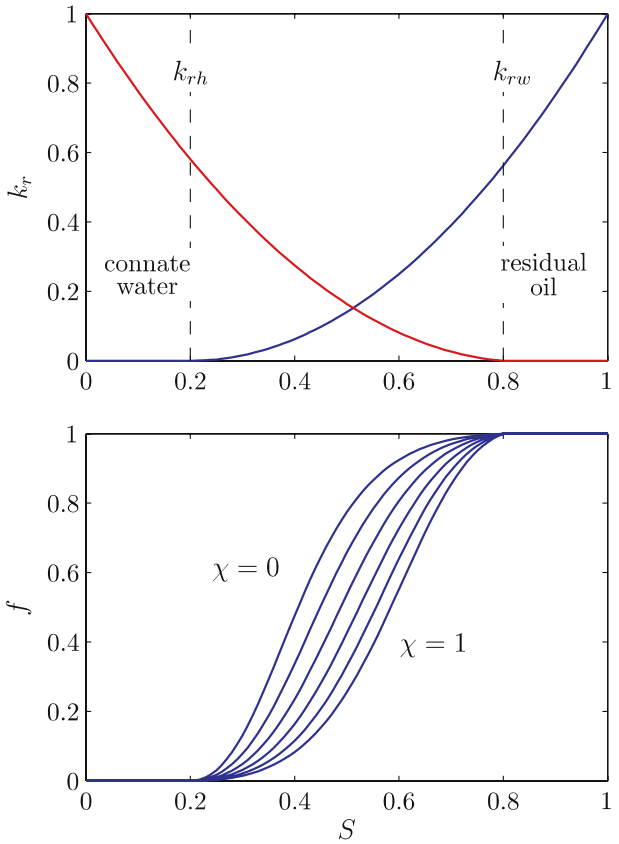

Figure 2. Top: relative permeabilities of the water and hydrocarbon phases. Bottom: dependence of the fractional flow function on the solvent mass fraction.

Since the hydrocarbon viscosity decreases with the solvent fraction, the overall mobility of the hydrocarbon phase is enhanced, resulting in lower values of the water fractional flow. The dependence of the fractional flow function on the solvent mass fraction is illustrated in Figure 2.

The effects of viscous fingering are incorporated by an empirical model that modifies the effective solvent flux in such a way that the dispersive effect of viscous fingering is captured:

$$(1-f)\frac{C}{1-S} \equiv (1-f)\chi \quad \longrightarrow \quad (1-f)g. \tag{10}$$

In Figure 3 we show a schematic diagram of a stable and an unstable miscible, single-phase displacement. Macroscopic models of viscous fingering introduce the solvent flux function g in an attempt to capture the *averaged* solvent mass fraction with a one-dimensional advective model (Koval, 1963).

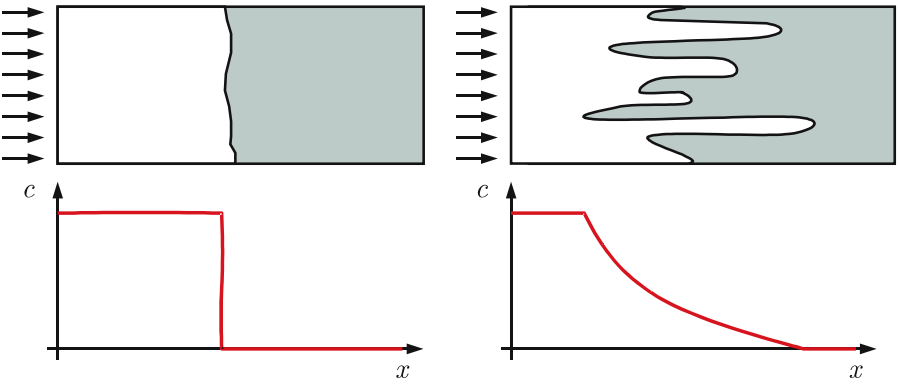

Figure 3. Schematic diagram of a stable miscible displacement (left) and an unstable miscible displacement (right) of oil by solvent.

In this work, we shall use the solvent flux function (fractional flow of solvent within the hydrocarbon phase) proposed by Koval (1963) and Todd and Longstaff (1972):

$$g = \hat{g}(\chi) = \frac{\chi}{\chi + \dfrac{1-\chi}{M_{\text{eff}}}}, \tag{11}$$

where M_{eff} is the effective mobility ratio. It is equal to one if viscous fingering is not present, and increases as viscous fingering effects become more pronounced. Different models exist to predict the value of M_{meff} given the oil and solvent viscosities. For example, Koval (1963) proposed

$$M_{\text{eff}} = \left(0.78 + 0.22 M^{1/4}\right)^4, \tag{12}$$

and Todd and Longstaff (1972) suggested

$$M_{\text{eff}} = M^{1-\omega} \tag{13}$$

with $\omega = 2/3$. Both correlations produce good agreement with experimental results for single-phase miscible displacements. In this paper we have used the solvent flux function proposed by Koval. We have chosen Koval's model because it does not require calibration of an extra parameter, and produced better agreement with experimental data (Blackwell *et al.*, 1959) than the Todd and Longstaff model with a single value of the parameter ω (Fayers *et al.*, 1992; Blunt and Christie, 1993). In Figure 4 we plot this function for an oil–solvent viscosity ratio $M = 10$, for which the effective mobility ratio is $M_{\text{eff}} \approx 1.88$.

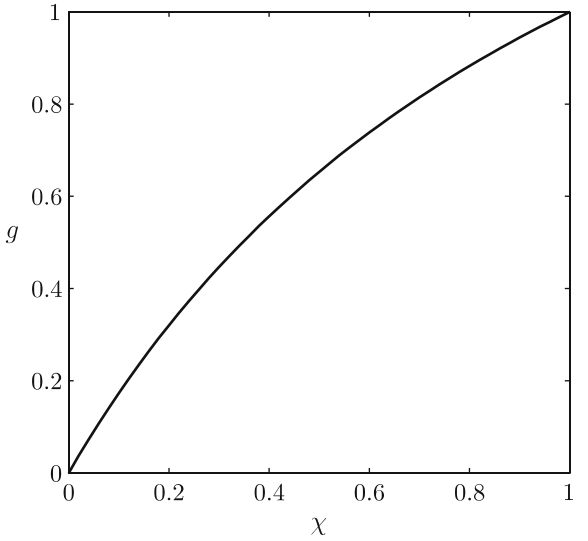

Figure 4. Solvent fractional flow function proposed by Koval (1963) for an effective mobility ratio $M_{\text{eff}} \approx 1.88$.

3. Character of the System of Equations

A detailed analysis of the mathematical character of the equations for the miscible system with no viscous fingering is given in Juanes and Lie (2005), and will not be repeated here. When the effect of viscous fingering is incorporated, the system of conservation equations takes the following form:

$$\partial_t \begin{bmatrix} S \\ C \end{bmatrix} + \partial_x \begin{bmatrix} f \\ (1-f)g \end{bmatrix} = \begin{bmatrix} 0 \\ 0 \end{bmatrix}, \tag{14}$$

where f and g are understood as functions of the conservation variables: $f = f(S, C)$ and $g = g(S, C)$. The solution vector (S, C) is restricted to lie on the unit triangle:

$$\mathcal{U} \equiv \{(S, C) : S \geq 0, \;\; C \geq 0, S + C \leq 1\}. \tag{15}$$

For some of the analysis that follows, it proves useful to use the relation between the solvent concentration and the solvent mass fraction given by Equation (3), and express the system (14) in terms of the nonconservation variables (S, χ):

$$\partial_t \begin{bmatrix} S \\ (1-S)\chi \end{bmatrix} + \partial_x \begin{bmatrix} f \\ (1-f)g \end{bmatrix} = \begin{bmatrix} 0 \\ 0 \end{bmatrix}, \tag{16}$$

where now f and g are understood as functions of the nonconservation variables: $f(S, C) = \hat{f}(S, \chi)$ and $g(S, C) = \hat{g}(\chi)$.

3.1. MATHEMATICAL CHARACTER

For smooth solutions, the system (14) can be written as

$$\partial_t \begin{bmatrix} S \\ C \end{bmatrix} + A(S,C)\partial_x \begin{bmatrix} S \\ C \end{bmatrix} = \begin{bmatrix} 0 \\ 0 \end{bmatrix}, \tag{17}$$

where A is the Jacobian matrix of the system:

$$A(S,C) := \begin{bmatrix} \frac{\partial f}{\partial S} & \frac{\partial f}{\partial C} \\ (1-f)\frac{\partial g}{\partial S} - \frac{\partial f}{\partial S}g & (1-f)\frac{\partial g}{\partial C} - \frac{\partial f}{\partial C}g \end{bmatrix}. \tag{18}$$

Alternatively, the quasi-linear form of the system of equations may be written in terms of the nonconservation variables by use of the chain rule:

$$\partial_t \begin{bmatrix} S \\ \chi \end{bmatrix} + \hat{A}(S,\chi)\partial_x \begin{bmatrix} S \\ \chi \end{bmatrix} = \begin{bmatrix} 0 \\ 0 \end{bmatrix}, \tag{19}$$

where

$$\hat{A}(S,\chi) := \begin{bmatrix} \frac{\partial \hat{f}}{\partial S} + \frac{\chi}{1-S}\frac{\partial \hat{f}}{\partial \chi} & \frac{1}{1-S}\frac{\partial \hat{f}}{\partial \chi} \\ \chi\frac{1-\hat{f}}{1-S}\frac{\partial \hat{g}}{\partial \chi} - \frac{\partial \hat{f}}{\partial S}\hat{g} - \chi\frac{\partial \hat{f}}{\partial \chi}\frac{\hat{g}}{1-S} & \frac{1-\hat{f}}{1-S}\frac{\partial \hat{g}}{\partial \chi} - \frac{\partial \hat{f}}{\partial \chi}\frac{\hat{g}}{1-S} \end{bmatrix}. \tag{20}$$

The local character of the system is determined by the eigenvalues (ν_1 and ν_2) and eigenvectors (r_1 and r_2) of the Jacobian matrix (Zauderer, 1983). The system is hyperbolic if the eigenvalues are real, and strictly hyperbolic if the eigenvalues are real and distinct. In the latter case, the matrix is diagonalizable and there exist two real and linearly independent eigenvectors. If the two eigenvalues are complex conjugates, the system is said to be elliptic.

If we express the 2×2 Jacobian matrix (20) in the generic form

$$\hat{A} = \begin{bmatrix} a & b \\ c & d \end{bmatrix}, \tag{21}$$

the eigenvalues of the system are given by:

$$\nu_{1,2} = \frac{1}{2}\left[(a+d) \mp \sqrt{\Delta}\right], \tag{22}$$

where

$$\Delta = (a-d)^2 + 4bc. \tag{23}$$

The eigenvalues are the characteristic speeds of propagation of waves and the eigenvectors are the corresponding characteristic directions in phase space. The system is hyperbolic if $\Delta \geq 0$ and strictly hyperbolic if the

inequality is strict. In our case, and after some algebraic manipulations, the discriminant is given by

$$\Delta = \left[\frac{\partial \hat{f}}{\partial S} - \frac{1-\hat{f}}{1-S}\frac{\partial \hat{g}}{\partial \chi} - \frac{\partial \hat{f}}{\partial \chi}\frac{\hat{g}-\chi}{1-S} \right]^2 - 4\frac{\partial \hat{f}}{\partial \chi}\frac{\hat{g}-\chi}{1-S}\frac{1-\hat{f}}{1-S}\frac{\partial \hat{g}}{\partial \chi}. \tag{24}$$

Equation (24) deserves some attention. The term in brackets is squared and is always nonnegative. Since the water fractional flow and the solvent flux functions satisfy the following conditions:

$$0 \le \hat{f} \le 1, \quad \frac{\partial \hat{f}}{\partial \chi} \le 0, \quad \chi \le \hat{g} \le 1, \quad \frac{\partial \hat{g}}{\partial \chi} > 0, \tag{25}$$

the second term in Equation (24) is always nonnegative also. Therefore, the system is everywhere hyperbolic. However, it is not strictly hyperbolic for certain composition states:

1. In the region of residual hydrocarbon saturation, $S > 1 - S_{hc}$. In this region, $\hat{f} \equiv 1$ and the discriminant is identically equal to zero. In fact, the Jacobian matrix is the zero matrix, so both eigenvalues are equal to zero and every direction is characteristic.
2. For particular states on the oil–water edge ($\chi = 0$) and the solvent–water edge ($\chi = 1$) of the saturation triangle. Along these edges, $\hat{g} = \chi$ and the discriminant simplifies to

$$\Delta = \left[\frac{\partial \hat{f}}{\partial S} - \frac{1-\hat{f}}{1-S}\frac{\partial \hat{g}}{\partial \chi} \right]^2. \tag{26}$$

The solvent flux function (11) satisfies

$$\left.\frac{\partial \hat{g}}{\partial \chi}\right|_{\chi=0} = M_{\text{eff}}, \qquad \left.\frac{\partial \hat{g}}{\partial \chi}\right|_{\chi=1} = \frac{1}{M_{\text{eff}}}. \tag{27}$$

On each edge, there is a single saturation state for which $\Delta = 0$. For that saturation state on the oil–water edge ($\chi = 0$), the Jacobian matrix reduces to

$$\hat{A}(S,\chi) := \begin{bmatrix} \frac{\partial \hat{f}}{\partial S} & \frac{1}{1-S}\frac{\partial \hat{f}}{\partial \chi} \\ 0 & \frac{1-\hat{f}}{1-S}M_{\text{eff}} \end{bmatrix}. \tag{28}$$

The double eigenvalue is $\nu = \frac{1-f}{1-S}M_{\text{eff}}$. The matrix is not diagonalizable, which means that the system is parabolic and there is one single characteristic direction on the (S, C)-plane, $r = (1, 0)$. For the nonstrictly

hyperbolic state on the solvent–water edge ($\chi = 1$), the Jacobian matrix takes the following expression:

$$\hat{A}(S,\chi) := \begin{bmatrix} \frac{\partial \hat{f}}{\partial S} + \frac{1}{1-S}\frac{\partial \hat{f}}{\partial \chi} & \frac{1}{1-S}\frac{\partial \hat{f}}{\partial \chi} \\ -\frac{1}{1-S}\frac{\partial \hat{f}}{\partial \chi} & \frac{1-\hat{f}}{1-S}\frac{1}{M_{\text{eff}}} - \frac{1}{1-S}\frac{\partial \hat{f}}{\partial \chi} \end{bmatrix}. \tag{29}$$

The double eigenvalue is $v = \frac{1-f}{1-S}\frac{1}{M_{\text{eff}}}$. Again, the matrix is not diagonalizable and the double eigenvector on the (S, C)-plane is $r = (1, -1)$.

We are interested in the solution of the Riemann problem associated with the system of equations (14). Using vector notation, the problem consists in finding a weak solution to the system of hyperbolic conservation laws:

$$\partial_t u + \partial_x F = 0, \quad -\infty < x < \infty, \quad t > 0 \tag{30}$$

with the following initial conditions:

$$u(x,0) = \begin{cases} u_l & \text{if } x < 0, \\ u_r & \text{if } x \geq 0. \end{cases} \tag{31}$$

The state $u_l = (S_l, C_l)$ is the 'left' or 'injected' state, and $u_r = (S_r, C_r)$ is the 'right' or 'initial' state. The system of Equations (30) and the initial condition (31) are invariant under uniform stretching of coordinates $(x,t) \mapsto (cx, ct)$, $c > 0$. The solution must consist of centered waves emanating from the origin $(x,t) = (0,0)$. Therefore, we seek a self-similar solution

$$u(x,t) = U(\zeta), \tag{32}$$

where the similarity variable is $\zeta = x/t$. In what follows we describe key elements that allow to characterize the different waves that may arise in the solution.

3.2. INTEGRAL CURVES AND RAREFACTIONS

If the solution $U(\zeta)$ is smooth, it must satisfy (Smoller, 1994)

$$A(U)U' = \zeta U', \tag{33}$$

that is, ζ is an eigenvalue (v_1 or v_2) and U' is the corresponding eigenvector (r_1 or r_2). Therefore, smooth waves (rarefactions) must lie on an integral curve of the right eigenvectors. States U along an integral curve are defined by the differential equation

$$\frac{\mathrm{d}U}{\mathrm{d}\tau} = r_i(U(\tau)), \quad i = 1, 2. \tag{34}$$

The two families of integral curves (composition paths) are shown in Figure 5. Additionally, admissible rarefactions connecting two states must satisfy that the characteristic velocity $\zeta = x/t = \nu_1$ or ν_2 increases along the integral curve from the left state to the right state.

3.3. HUGONIOT LOCI AND SHOCKS

If the solution is discontinuous, states on opposite sides of the discontinuity must satisfy an integral version of the conservation equations, known as the Rankine–Hugoniot conditions. The set of states u that can be joined to a reference state $\hat{u}$ by a discontinuity must satisfy:

$$F(u) - F(\hat{u}) = \sigma \ (u - \hat{u}), \tag{35}$$

where σ is the speed of propagation of the discontinuity.

Locally, in a neighborhood of the reference state, Equation (35) admits two families of solutions, associated with the slow and fast eigenvalues. These two sets of solutions define the *local* branches of the Hugoniot locus.

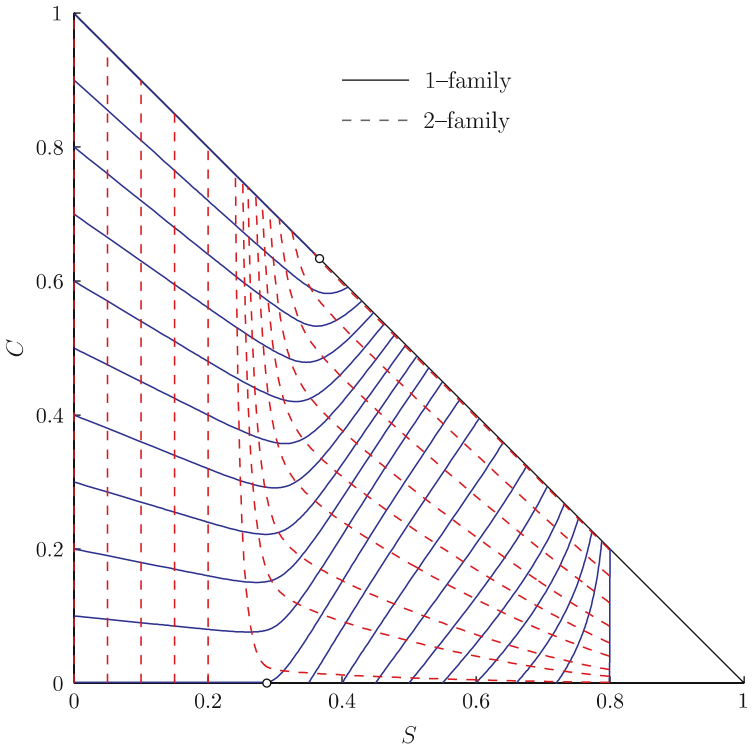

Figure 5. Integral curves of the 1-family (blue) and 2-family (red) on the ternary diagram. The two circles (○) correspond to states where the system is nonstrictly hyperbolic.

In general, Hugoniot loci and integral curves locally have second-order tangency (Smoller, 1994).

Not all states in the Hugoniot locus can be joined to the reference state through a physically admissible discontinuity. A shock must satisfy additional entropy conditions to be physically valid. Entropy conditions for strictly hyperbolic systems were compiled by Lax (1957) and extended by Liu (1974, 1975) into what is now known as e-Lax admissibility criterion. The development of suitable entropy conditions for nonstrictly hyperbolic systems is still an open issue. A large body of literature has emerged in an attempt to develop conditions that guarantee existence and uniqueness of the solution (Schaeffer and Shearer, 1987a, b; Marchesin and Plohr, 2001).

In this work, we find unique solutions to the Riemann problem that satisfy the e-Lax entropy criterion. Therefore, a valid discontinuity that joins states u and $\hat{u}$ may be a *1-Lax shock* if it satisfies:

$$\begin{aligned} v_1(u) \geq \sigma &\geq v_1(\hat{u}), \\ \sigma &< v_2(\hat{u}), \end{aligned} \tag{36}$$

or a *2-Lax shock* if it satisfies:

$$\begin{aligned} v_2(u) \geq \sigma &\geq v_2(\hat{u}), \\ v_1(u) &< \sigma. \end{aligned} \tag{37}$$

A common feature of systems of conservation laws describing multiphase flow is the existence of *detached* branches of the Hugoniot locus (Barkve, 1989; da Mota, 1992; de Souza, 1992; Falls and Schulte, 1992; Isaacson *et al.*, 1992; Marchesin and Plohr, 2001). These consist of states which satisfy the Rankine–Hugoniot conditions, but do not belong to the local branches that emanate from the reference state. In Figure 6 we plot the Hugoniot locus for a reference state $\hat{u} = (0.2, 0)$ that corresponds to a secondary flood. In addition to the local branches associated with a slow shock (along the line $C = 0$) and a fast shock (line $S = 0.2$), there is a detached branch of states that satisfy the Rankine–Hugoniot conditions. This set of states, however, does not satisfy the Lax entropy conditions and does not play a role in the construction of solutions. In Figure 7 we show the Hugoniot locus for a reference state $\hat{u} = (0.8, 0)$. As before, the two local branches are $C = 0$ (slow shock) and $S = 0.8$ (fast shock). A detached branch also exists, which corresponds to admissible 2-Lax shocks. As we discuss in Section 4, the presence of this detached branch is essential in the construction of analytical solutions for tertiary floods.

3.4. INFLECTION LOCI AND RAREFACTION–SHOCKS

The two characteristic fields of the system (14) are neither genuinely nonlinear nor linearly degenerate in the sense of Lax (1957). A field is said

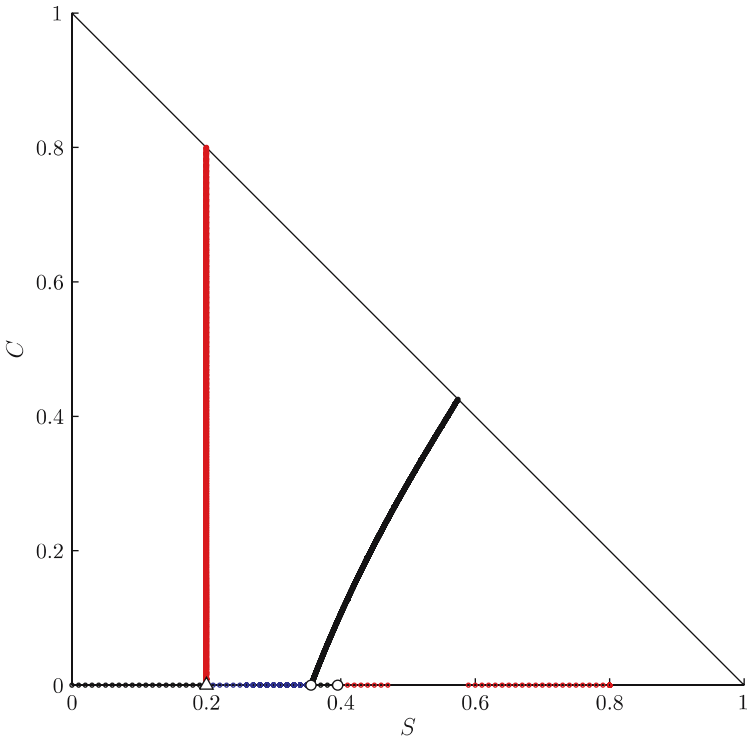

Figure 6. Hugoniot loci for a reference state $\hat{u} = (0.2, 0)$ ($\triangle$) corresponding to a secondary flood.

to be genuinely nonlinear if eigenvalues vary monotonically along integral curves. A field is linearly degenerate if eigenvalues are constant along integral curves of a particular characteristic family. In our case, however, eigenvalues attain a local extremum along integral curves. The local extrema of the i-family satisfy the following condition:

$$\nabla v_i \cdot r_i = 0. \tag{38}$$

The locus of states for which Equation (38) is satisfied is known as the i-inflection locus (Johansen and Winther, 1988; Schecter *et al.*, 1996; Ancona and Marson, 2001). In Figures 8 and 9 we plot the inflection loci of the 1- and 2-characteristic families, respectively, along with the contours of the corresponding eigenvalues. The relevance of inflection loci stems from the fact that an admissible rarefaction cannot be extended across the inflection locus of the associated family. For genuinely nonlinear systems, individual waves may only be rarefactions or shocks (Lax, 1957). However, for systems that are not genuinely nonlinear, such as the Buckley–Leverett equation, individual waves may involve both (Liu, 1974). When inflection loci are single, connected curves a wave may only be a combination

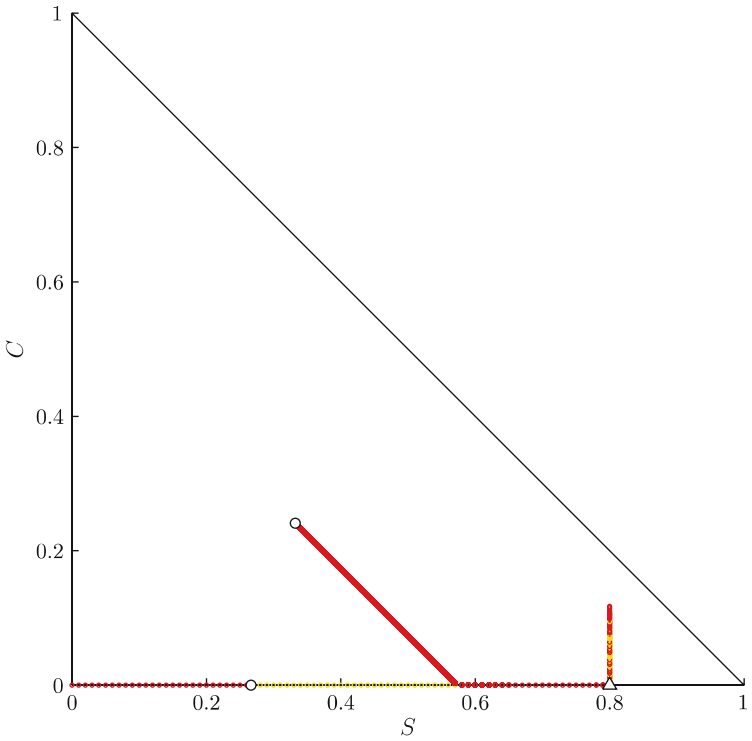

Figure 7. Hugoniot loci for a reference state $\hat{u} = (0.8, 0)$ ($\triangle$) corresponding to a tertiary flood.

of one rarefaction and one shock. If, in addition, inflection loci correspond to *maxima* of eigenvalues, the rarefaction is always slower than the shock (Ancona and Marson, 2001). This property was employed extensively in the development of a complete Riemann solver for three-phase immiscible flow (Juanes and Patzek, 2004; Juanes, 2005).

4. Analytical Solutions

We develop analytical solutions to the Riemann problem (30)–(31) for two cases of interest: secondary floods and tertiary floods. In the case of secondary floods, we consider injection of a water–solvent mixture into a medium that contains oil and connate water. A tertiary flood refers to the case when the water–solvent mixture is injected into a reservoir that has previously been waterflooded to residual oil saturation. Therefore, our analysis is restricted to initial states along the oil–water edge ($C = 0$) and to injected states along the water–solvent edge ($C = 1 - S$). Although we do not anticipate major difficulties in developing a full catalogue and classifi-

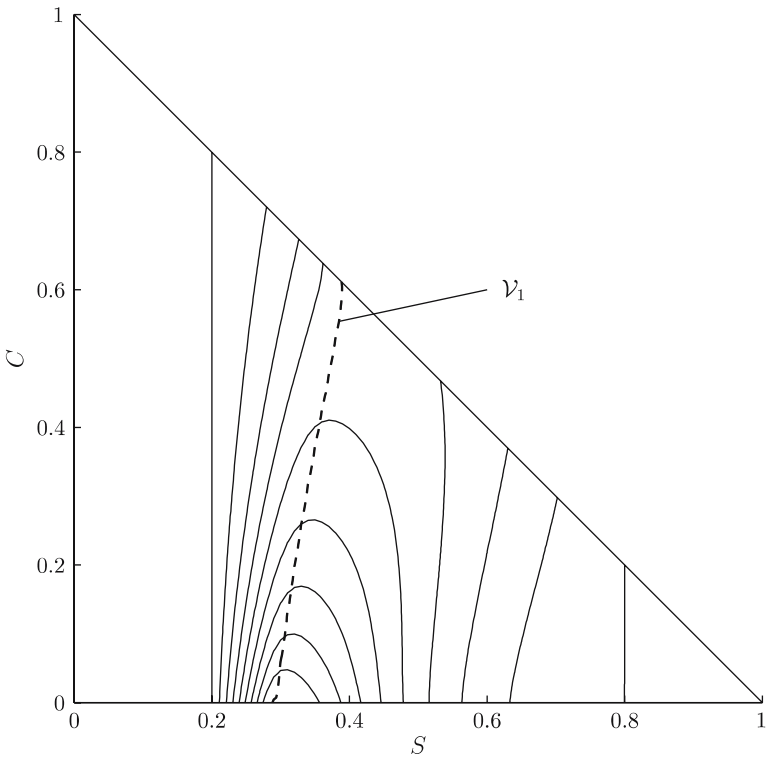

Figure 8. Isocontours of eigenvalues of the 1-family, and the corresponding inflection locus.

cation of solutions for *any* initial and injected states, the complete Riemann solver is not presented here.

Our analysis in this section is restricted to using the *nominal* value of the effective mobility ratio M_{eff} given by Equation (12). No attempt was made to adapt M_{eff} in a self-consistent fashion (Blunt and Christie, 1993, 1994). However, even if the effective mobility ratio is adapted dynamically depending on the mobility drop across a solvent front, the global structure of the solution for tertiary floods is still similar to that presented here and still involves the detached branch of the Hugoniot locus. We discuss and illustrate this point in Section 5.3.

We use the Lax entropy criterion for the construction of our solutions. Therefore, solutions are obtained as a sequence of a slow 1-wave and a fast 2-wave, which are connected at an intermediate constant state:

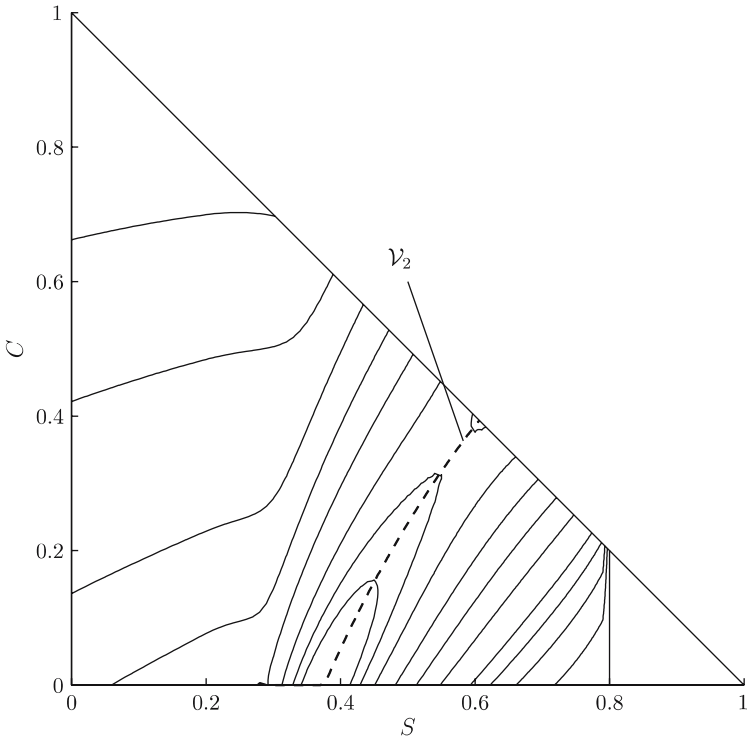

Figure 9. Isocontours of eigenvalues of the 2-family, and the corresponding inflection locus.

$$u_l \xrightarrow{\mathcal{W}_1} u_m \xrightarrow{\mathcal{W}_2} u_r. \tag{39}$$

Each of the two waves ($i = 1, 2$) may be a rarefaction $\mathcal{R}_i$, a shock $\mathcal{S}_i$, or a rarefaction–shock $\mathcal{R}_i\mathcal{S}_i$. We obtain unique admissible solutions using this entropy criterion (at least for the cases considered below). Some of the solutions involve detached branches of the shock curves in an essential way.

In the discussion that follows, a comparison is performed between the analytical solution and a one-dimensional numerical solution. In all cases, we used a single-point upstream finite-difference method, with an explicit Forward Euler time integration scheme. The numerical solutions were computed on a grid of 1000 cells and a time step of $\delta t = 0.00025$, corresponding to a CFL number of about 0.5 for most of the cases presented. From numerical experiments with different grid resolutions (keeping the CFL number constant), it appears that the numerical simulations reflect converged solutions.

4.1. SECONDARY FLOODS

We consider the initial state $u_r = (S_r, C_r) = (0.2, 0)$, that is, an oil–water system at connate water saturation, and different injection states.

Case I. The first case we consider is that of pure solvent injection, $u_l = (S_l, C_l) = (0, 1)$. The solution, shown in Figure 10, consists of a slow rarefaction $\mathcal{R}_1$ (in fact, a contact discontinuity of zero speed), and a long fast rarefaction $\mathcal{R}_2$ associated with the dispersed solvent front. This solution displays the basic feature of the viscous fingering model: the fast solvent front, which would be a sharp contact discontinuity if fingering effects are ignored (Juanes and Lie, 2005), is now a smooth rarefaction with a ratio between its maximum and minimum speeds equal to M_{eff}^2 where $M_{\text{eff}} \approx 1.88$. On the left plot of Figure 10 we show the composition path corresponding to the analytical solution (solid line) and the numerical solution (dotted line – superimposed to the solid line in this case and therefore barely visible). Also shown are the inflection loci of the slow and fast families (dashed lines). On the right plot of Figure 10 we show the corresponding composition profile. We plot the profiles of water saturation S (solid line) and solvent mass fraction χ (dashed line) against the self-similarity variable ζ. Also shown with circles connected by a dotted line is the numerical solution obtained by single-point upstream finite differences. Because of the large number of points, these lines often look like thick solid lines. The agreement between the analytical and numerical solutions is excellent.

Case II. Next we consider the case when a mixture of water and solvent is injected, with a water saturation greater than the connate water saturation: $u_l = (0.4, 0.6)$. The solution is now made up of a slow 1-Lax shock $\mathcal{S}_1$ at constant solvent mass fraction, and the same fast rarefaction $\mathcal{R}_2$ as in

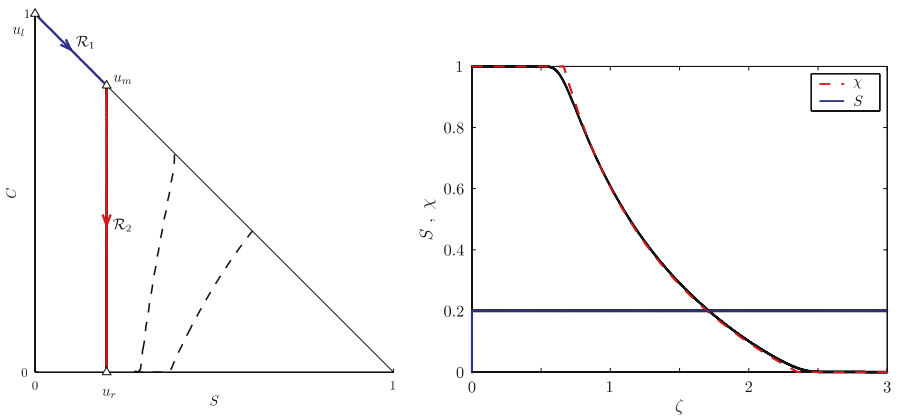

Figure 10. Secondary flood. Case I: injection state $(S, C) = (0, 1)$.

the previous case (see Figure 11). Since the water shock lags behind the solvent front and does not interact with it, the injection scheme is not more efficient than that of Case I, but requires less solvent.

Case III. If one injects a water–solvent mixture with a higher proportion of water, the composition path of the slow wave is no longer along the the water–solvent edge. In Figure 12 we show the analytical solution when the injected state is $u_I = (0.5, 0.5)$. The solution still presents a fast rarefaction, but its amplitude is reduced compared with the previous two cases. The reason is that the slow wave intersects the fast rarefaction at an intermediate state that is not on the water–solvent edge. Notice that the slow wave is a rarefaction–shock $\mathcal{R}_1\mathcal{S}_1$ that crosses the 1-inflection locus.

Case IV. If the ratio of water to solvent injected is sufficiently high, the slow wave is a single rarefaction associated with the solvent front that lags behind a classical Buckley–Leverett shock. One such case is shown in Fig-

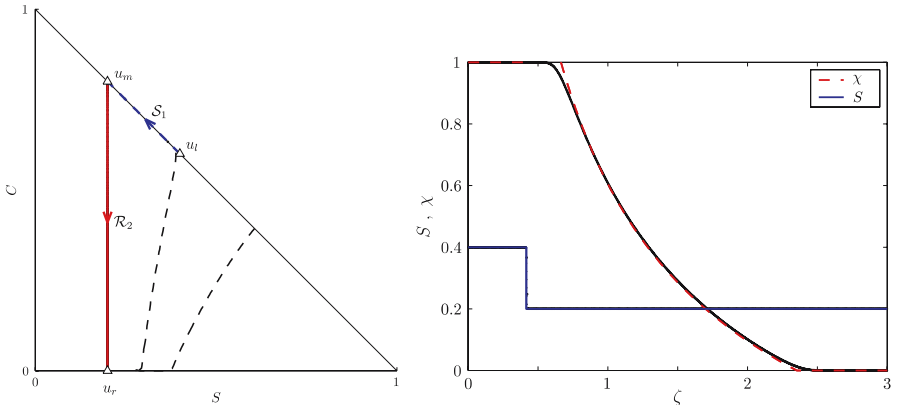

Figure 11. Secondary flood. Case II: injection state $(S, C) = (0.4, 0.6)$.

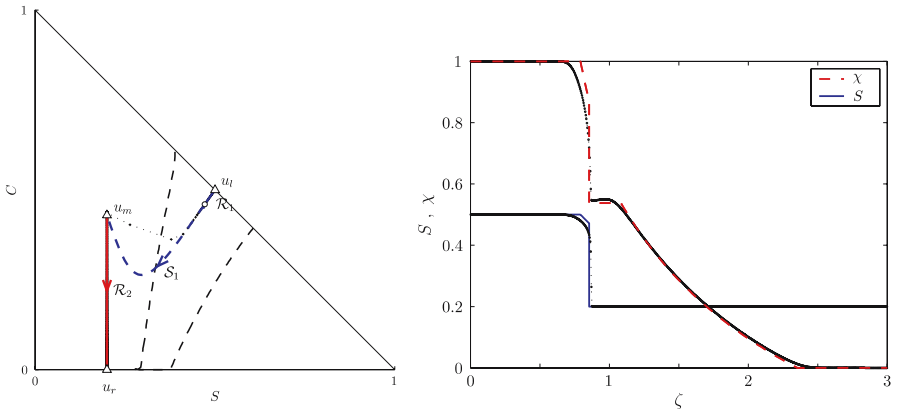

Figure 12. Secondary flood. Case III: injection state $(S, C) = (0.5, 0.5)$.

ure 13 for an injected state $u_l = (0.65, 0.35)$. One can conclude that there is an optimum ratio of water to solvent injected (Stalkup, 1983; Blunt and Christie, 1993) that would lie between Cases III and IV, and for which the leading edge of the solvent front and the water front would travel at the same speed.

4.2. TERTIARY FLOODS

We consider the initial state $u_r = (S_r, C_r) = (0.8, 0)$, that is, an oil–water system at residual oil saturation. We study the different solution types that emerge as we vary the water–solvent ratio of the injected fluid.

Case I. Pure solvent is injected into the medium, that is, $u_l = (0, 1)$. The solution comprises two waves: a slow rarefaction $\mathcal{R}_1$ along the water–solvent edge (constant solvent mass fraction $\chi = 1$), and a fast rarefaction–shock $\mathcal{R}_2\mathcal{S}_2$ (Figure 14). The essential ingredient in the construction of the solution is that the rarefaction and the shock join at a state that belongs to the detached branch of the Hugoniot locus of the initial state (see Figure 7). This is one of the distinct features that characterizes our solutions to tertiary WAG flooding. This solution is fundamentally different from the ones presented in Blunt and Christie (1993), where the initial condition considered was such that the solvent front would not interact with a leading Buckley–Leverett shock, so the solution would not involve the detached branch. In our case, on the other hand, the fast wave embodies simultaneous changes of both water saturation and solvent mass fraction. The solution constructed in this way is the unique solution that satisfies the Lax entropy criterion. Moreover, we show at the end of this section that the leading shock is stable to viscous fingering and, therefore, consistent with our model description.

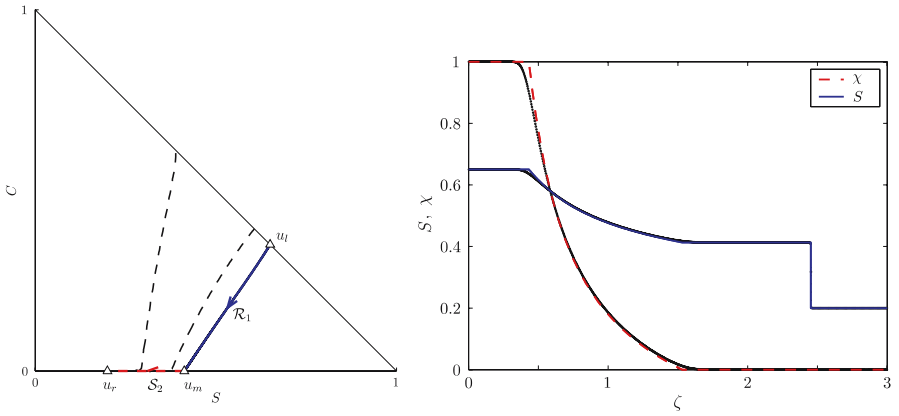

Figure 13. Secondary flood. Case IV: injection state $(S, C) = (0.65, 0.35)$.

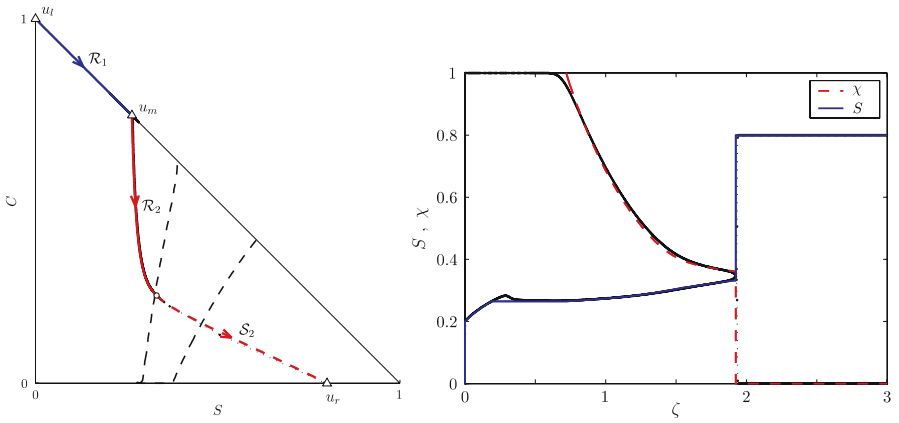

Figure 14. Tertiary flood. Case I: injection state $(S, C) = (0, 1)$.

Case II. If the injected state is a water–solvent mixture with a low fraction of water (but higher than the connate water saturation), the solution is essentially the same as for Case I, except that the slow wave is a 1-Lax shock with constant solvent mass fraction $\chi = 1$ (Figure 15). The fast wave is identical to that of the previous case and, therefore, oil recovery is not more effective but requires less solvent.

Case III. When the injected mixture contains a higher proportion of water, the composition path of the slow wave does not follow the water–solvent edge. Shown in Figure 16 is the solution for $u_l = (0.47, 0.53)$. The slow wave is now a composite rarefaction–shock $\mathcal{R}_1\mathcal{S}_1$ that intersects the fast rarefaction–shock $\mathcal{R}_2\mathcal{S}_2$ at a state inside the ternary diagram. It is worth noting that both waves cross the inflection locus of their respective family. The amplitude and speed of the leading shock is the same as in

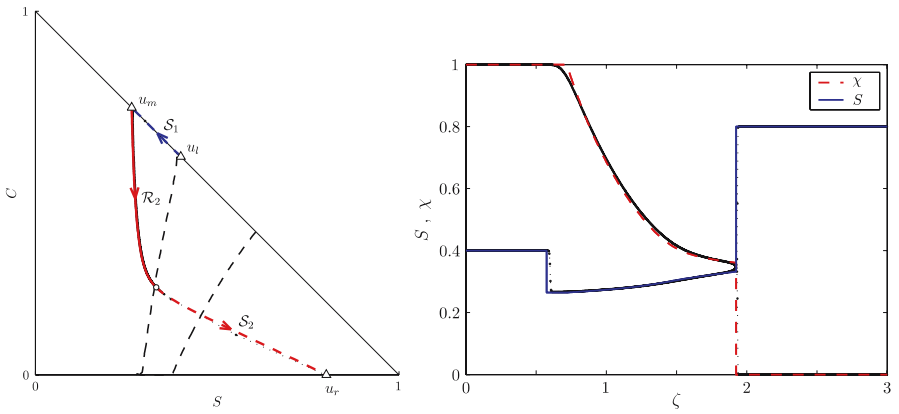

Figure 15. Tertiary flood. Case II: injection state $(S, C) = (0.4, 0.6)$.

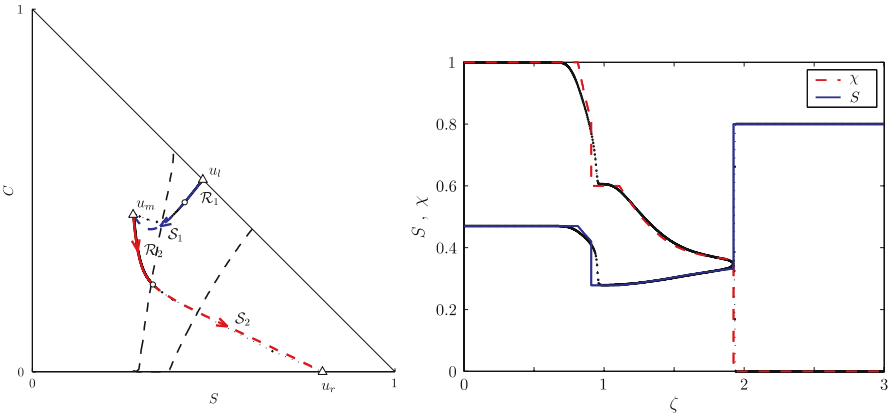

Figure 16. Tertiary flood. Case III: injection state $(S, C) = (0.47, 0.53)$.

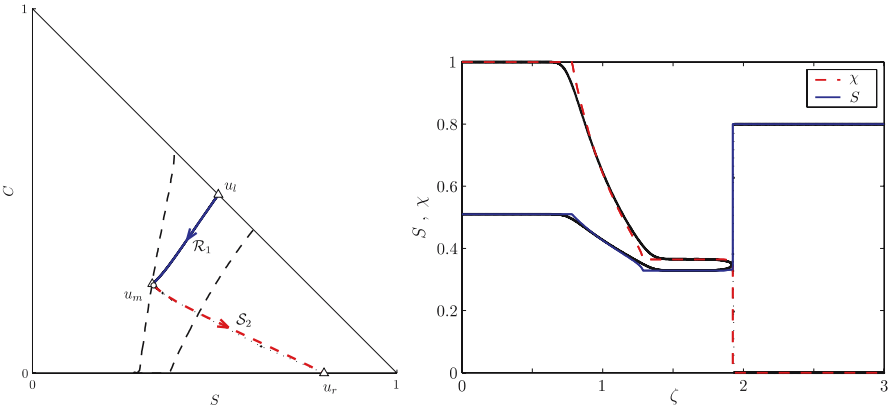

Figure 17. Tertiary flood. Case IV: injection state $(S, C) = (0.51, 0.49)$.

Cases I and II above, but the speed of the slow wave is higher, leading to a (slightly) more effective recovery scheme.

Case IV. For an injected state $u_l = (0.51, 0.49)$, the amplitude of the fast rarefaction $\mathcal{R}_2$ is minimized, while the amplitude of the leading shock $\mathcal{S}_2$ is maximized. The solution in this case, shown in Figure 17, consists of a slow rarefaction $\mathcal{R}_1$ and a fast rarefaction–shock $\mathcal{R}_2\mathcal{S}_2$ with a very small rarefaction. It is important to notice that both waves (the slow rarefaction and the fast shock) entail simultaneous changes in the volume fractions of all three fluids.

Case V. If the fraction of injected water is increased further, the amplitude and the speed of the leading shock are lower and the speed of the slow wave decreases also, resulting in a less effective recovery scheme. In Figure 18 we plot the solution for $u_l = (0.6, 0.4)$. The solution consists of

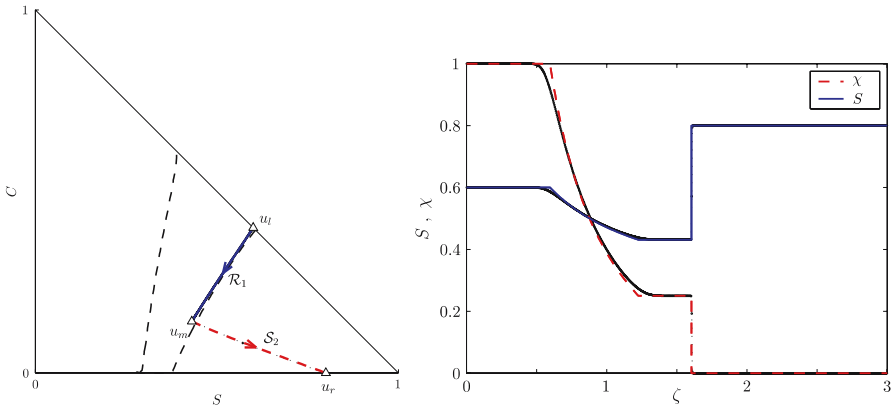

Figure 18. Tertiary flood. Case V: injection state $(S, C) = (0.6, 0.4)$.

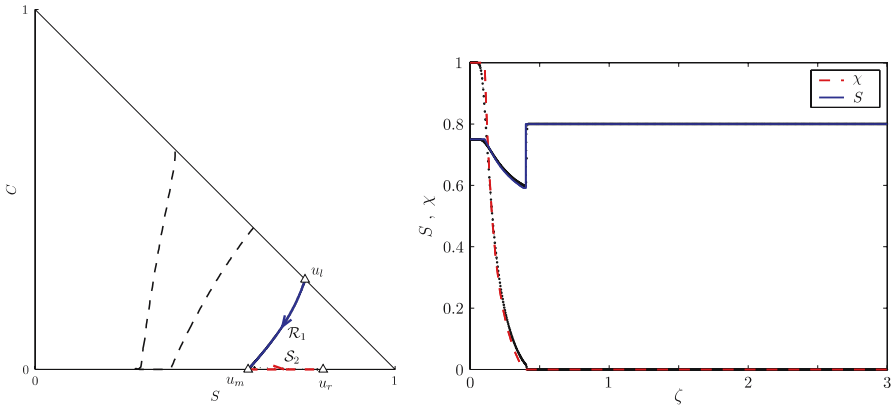

Figure 19. Tertiary flood. Case VI: injection state $(S, C) = (0.75, 0.25)$.

a slow rarefaction $\mathcal{R}_1$ and a fast shock $\mathcal{S}_2$, which join at an intermediate state on the detached branch.

Case VI. For very high water to solvent ratio, the analytical solution is still of type $\mathcal{R}_1\mathcal{S}_2$ as in Case V, but the slow rarefaction intersects with the local branch of the Hugoniot locus, rather than the detached branch. Therefore, the intermediate state is on the water–oil edge, as shown in Figure 19 for an injected state $u_l = (0.75, 0.25)$.

5. Discussion

In this section, we discuss further several important aspects of the analytical solutions presented above: (1) the need to consider the detached branch of the Hugoniot locus; (2) the influence of the viscous fingering model; (3) the extension of the analysis to use a self-consistent value of the effec-

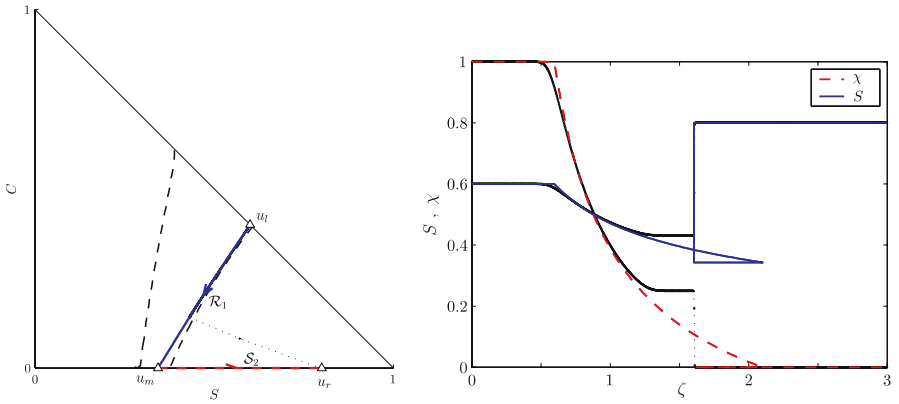

Figure 20. Wrong solution for a tertiary flood, in which the detached branch of the Hugoniot locus is not considered.

tive mobility ratio; and (4) the impact of viscous fingering on the prediction of the optimum WAG ratio.

5.1. ROLE OF DETACHED BRANCHES

It is apparent that the presence of a detached branch of the Hugoniot locus of the right state is essential for the construction of analytical solutions to tertiary floods. In Figure 20 we plot the solution that would be determined for an injected state $u_l = (0.6, 0.4)$ if one uses the local branches of the Hugoniot locus only. The solution is still of type $\mathcal{R}_1\mathcal{S}_2$, but the sequence of wave speeds is not monotonically increasing, and the global solution is clearly inadmissible. The fast shock connecting the intermediate state u_m with the right state u_r does not satisfy the Lax entropy criterion because even though the characteristics of the 2-family impinge onto the shock,

$$v_2(u_m) > \sigma > v_2(u_r), \tag{40}$$

the characteristic of the 1-family is faster than the shock:

$$v_1(u_m) > \sigma, \tag{41}$$

which violates conditions (37). This inadmissible solution should be compared with the correct entropy solution in Figure 18. For a reader who is familiar with fractional flow theory (Pope, 1980; Helfferich, 1981; Walsh and Lake, 1989), the presence of detached branches means that the solution *cannot* be constructed graphically from the water–oil and water–solvent fractional flow curves alone, because the leading shock involves changes in all three compositions.

The presence of admissible parts in the detached branches of the Hugoniot locus has also been observed in hyperbolic models of three-phase immiscible flow (Marchesin and Plohr, 2001; Isaacson *et al.*, 1992; de Souza, 1992; Falls and Schulte, 1992) and nonisothermal two-phase flow (Barkve, 1989; da Mota, 1992).

5.2. EFFECT OF THE VISCOUS FINGERING MODEL

The second aspect we want to emphasize is the influence of the viscous fingering model in the global structure of the solution. To illustrate this effect, we compare the analytical solutions for a tertiary flood of pure solvent injection predicted by the multiphase first-contact miscible model with and without viscous fingering. Such comparison is presented in Figure 21. On the left side of the figure we plot the composition path, the composition profiles and the mobility profile corresponding to the solution that does not account for viscous fingering (Juanes and Lie, 2005). The solution comprises two wave groups: (1) a slow wave group with a contact discontinuity and a slow rarefaction at constant solvent mass fraction $\chi = 1$; and (2) a fast wave group with a contact discontinuity describing the solvent front and a fast rarefaction-shock at constant solvent mass fraction $\chi = 0$. The mobility ratio across the solvent front is about 10, indicating that such front is unstable to viscous fingering.

The analytical solution for the model with viscous fingering is shown on the right side of Figure 21. The important point is that the effect of the viscous fingering model is not restricted to spreading out the solvent front. The solution now involves the detached branch of the Hugoniot locus, and the composition path is entirely different. Physically, this is related to the fact that the solvent front is dispersed to an extent that its leading edge interacts with the fast Buckley–Leverett shock. The consequence of this interaction is the presence of a genuine shock at the leading edge of the oil bank that involves changes of *both* water saturation and solvent mass fraction. From the mobility profile shown in the bottom-right plot of Figure 21, it is clear that this shock entails a favorable mobility contrast, that is, $\lambda_T^{\text{up}}/\lambda_T^{\text{down}} < 1$. Therefore, the leading edge of the oil bank is stable with respect to viscous fingering.

5.3. A SELF-CONSISTENT EFFECTIVE MOBILITY RATIO

The Todd and Longstaff model of viscous fingering was extended to multiphase-multicomponent flows in Blunt and Christie (1993, 1994), and Blunt *et al.* (1994). They used the same solvent flux function $\hat{g}(\chi)$, but dynamically calibrating the only parameter of the model, the effective mobility ratio M_{eff}.

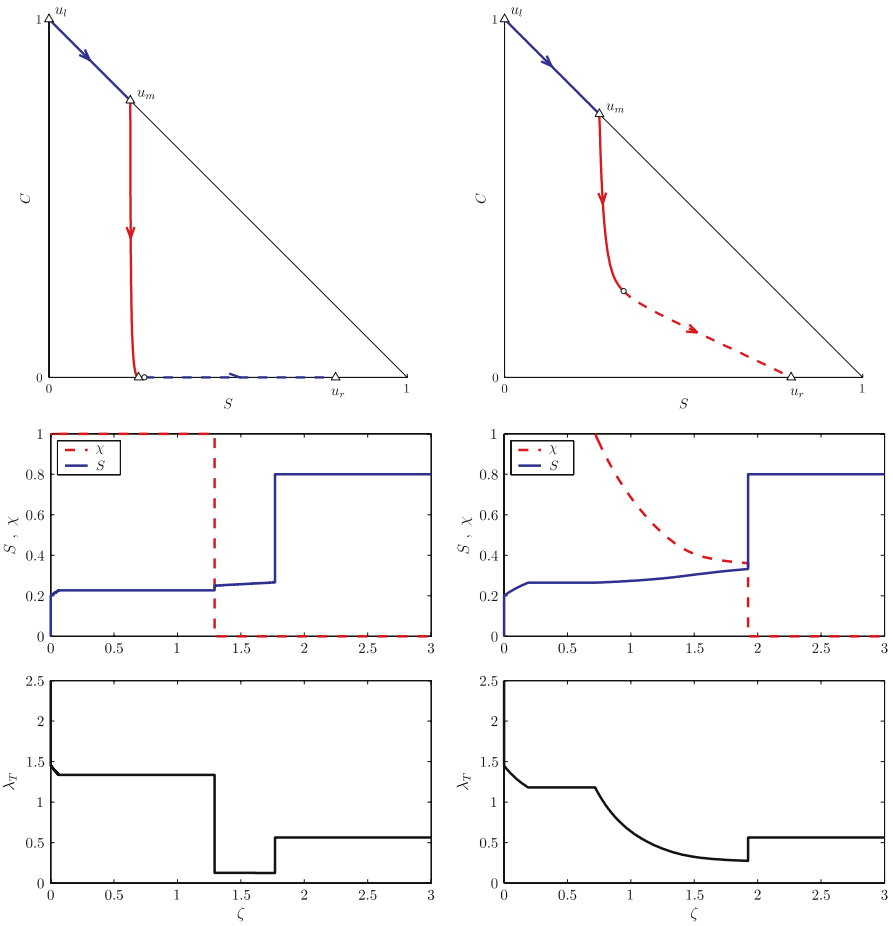

Figure 21. Comparison of the predictions for a tertiary flood of pure solvent. Left: no viscous fingering. Right: viscous fingering with nominal M_{eff}.

The premise is that the degree of fingering depends on the mobility contrast across the solvent front. For single-phase flows in which a first-contact miscible solvent is injected into an oil-filled medium, the mobility contrast M is equal to the viscosity ratio μ_o/μ_s. For multiphase flows, the mobility contrast is computed as the ratio of the total mobility immediately upstream and immediately downstream of the solvent front:

$$M = \frac{\lambda_T^{\text{up}}}{\lambda_T^{\text{down}}}. \tag{42}$$

The effective mobility ratio M_{eff} can then be calculated by inserting this value of M in Equation (12). Obviously, the value of the effective mobility ratio affects the solution, and so an iterative scheme is required to achieve

consistency between the *input* effective mobility ratio $M_{\text{eff}}^{\text{in}}$ and the *output* $M_{\text{eff}}^{\text{out}}$ obtained from Equations (42) and (12) once the solution is computed.

This type of consistency is missing from the solution given in Figure 21. The solution makes use of the nominal value of the mobility ratio, $M_{\text{in}} = 10$, which corresponds to $M_{\text{eff}}^{\text{in}} \approx 1.88$. The mobility contrast across the solvent front of the computed solution is $M_{\text{out}} \approx 4.32$, that is, $M_{\text{eff}}^{\text{out}} \approx 1.45$. Clearly, the nominal value of the mobility ratio is too large, which means that the degree of fingering is overestimated. The question is whether the structure of the solution persists if the correct value of M_{eff} is used. In particular, we want to know if the smearing of the solvent is sufficient to interact with the leading Buckley–Leverett shock.

The self-consistent value of M_{eff} was found by iteration. We used the secant method rather than the fixed-point iteration suggested in Blunt and Christie (1993) because of its much faster convergence. Given values of M_{in} at two iterations, and their corresponding values M_{out} obtained from the respective solutions, the new trial value of the mobility ratio is:

$$M_{\text{in}}^{(k+1)} = \frac{M_{\text{out}}^{(k-1)} - \alpha M_{\text{in}}^{(k-1)}}{1-\alpha}, \quad \text{where } \alpha = \frac{M_{\text{out}}^{(k)} - M_{\text{out}}^{(k-1)}}{M_{\text{in}}^{(k)} - M_{\text{in}}^{(k-1)}}. \tag{43}$$

The values of the input and output mobility ratios during the iterative process are reported in Table I.

The solution for the self-consistent value $M_{\text{in}} = M_{\text{out}} = 5.81$ ($M_{\text{eff}} \approx 1.58$) is shown in Figure 22. The important observation is that the degree of fingering is sufficient for the solvent front to interact with the leading Buckley–Leverett shock and, as a result, the solution involves the detached branch of the Hugoniot locus. Physically, this means that the solvent front pushes through and destroys the oil bank, resulting in a leading shock where both oil and solvent break through. This leading shock is stable.

Table I. Iteration towards a self-consistent value of the effective mobility ratio

Iter	M_{in}	($M_{\text{eff}}^{\text{in}}$)	M_{out}
0	10.000	(1.8817)	4.3161
1	4.3161	(1.4487)	7.7917
2	6.4729	(1.6357)	5.3758
3	5.9554	(1.5943)	5.7012
4	5.7993	(1.5814)	5.8179
5	5.8100	(1.5823)	5.8096

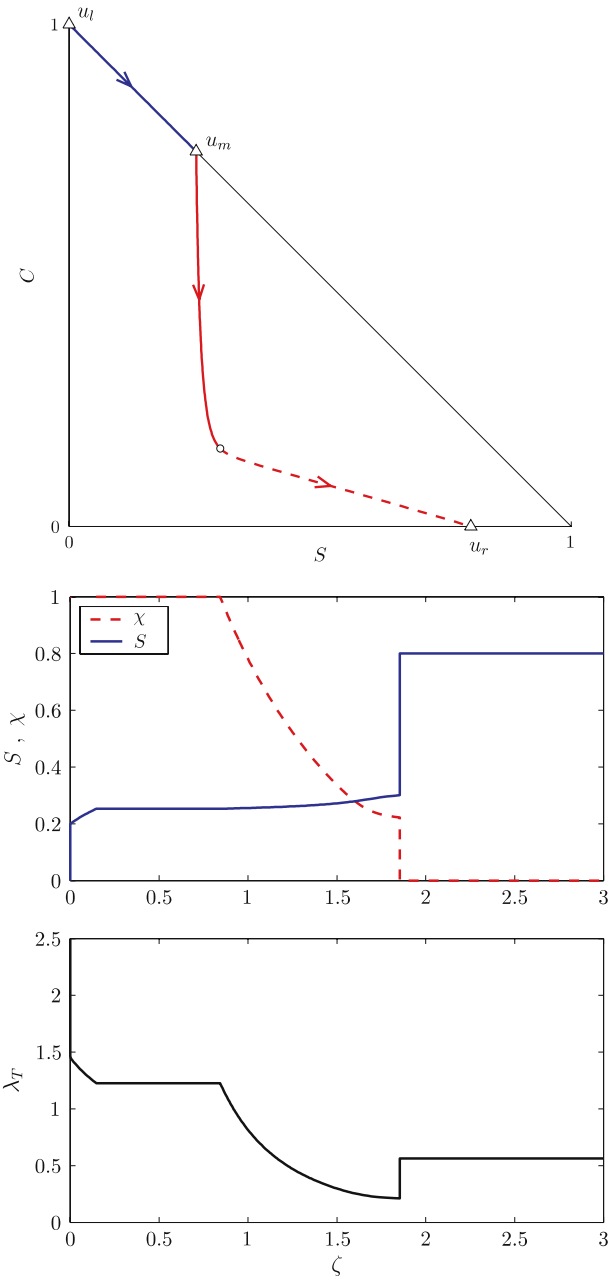

Figure 22. Predictions for a tertiary flood of pure solvent, using a viscous fingering model with a self-consistent value of the effective mobility ratio.

5.4. OPTIMUM WAG RATIO

The original motivation behind simultaneous injection of solvent and water was to limit the degree of fingering by reducing the mobility contrast between the injected and displaced fluids (Caudle and Dyes, 1958). The WAG ratio is defined as the ratio of injected water to injected solvent, both expressed in reservoir volumes:

$$W_R = \frac{f_{\text{inj}}}{1 - f_{\text{inj}}}, \tag{44}$$

where f_{inj} is the water fractional flow of the injected conditions. There is an optimum WAG ratio at which water and solvent fronts travel at the same speed, minimizing the degree of fingering and maximizing oil recovery. A graphical construction for the evaluation of the optimum WAG ratio in secondary and tertiary floods was first given by Stalkup (1983) when viscous fingering is not included in the analysis. An interesting application of fractional flow theory to miscible flooding was presented by Walsh and Lake (1989). They analyzed the effect of W_R on the displacement efficiency for both secondary and tertiary floods. Viscous fingering was not included, but they estimated the mobility contrast across the solvent front as a measure of the severity of fingering. The influence of the injected water–solvent ratio on displacement efficiency in the presence of viscous fingering was studied by Blunt and Christie (1993, 1994) using a self-consistent calibration of the effective mobility ratio. However, their analysis of tertiary floods was restricted to cases in which the solvent front would lag behind the leading edge of the oil bank.

In this section, we evaluate how the number of pore volumes injected (PVI) for 100% recovery and the mobility ratio across the solvent front vary with the WAG ratio. We restrict our attention to tertiary floods, but we cover the entire range of water–solvent ratios. Each individual solution has been obtained by iterating on the mobility ratio to achieve self-consistency as explained in Section 5.3. We also analyze how the new predictions compare with those when viscous fingering is not included (Walsh and Lake, 1989). The result of our analysis is shown in Figure 23. We plot the mobility ratio across the solvent front (top) and the number of PVI for 100% recovery (bottom) as a function of the injected water fractional flow f_{inj}.

The model *without* viscous fingering predicts that the displacement efficiency and the mobility ratio across the solvent front remain unchanged for $0 < f_{\text{inj}} < f_{\text{inj}}^{\text{crit}}$. At this critical $f_{\text{inj}}^{\text{crit}}$ the mobility ratio drops from a value of about 10 to a much lower value of about 4. For $f_{\text{inj}} > f_{\text{inj}}^{\text{crit}}$ the mobility ratio changes little, while the displacement efficiency decreases as W_R increases (more PVI are required to recover all the oil). The optimum

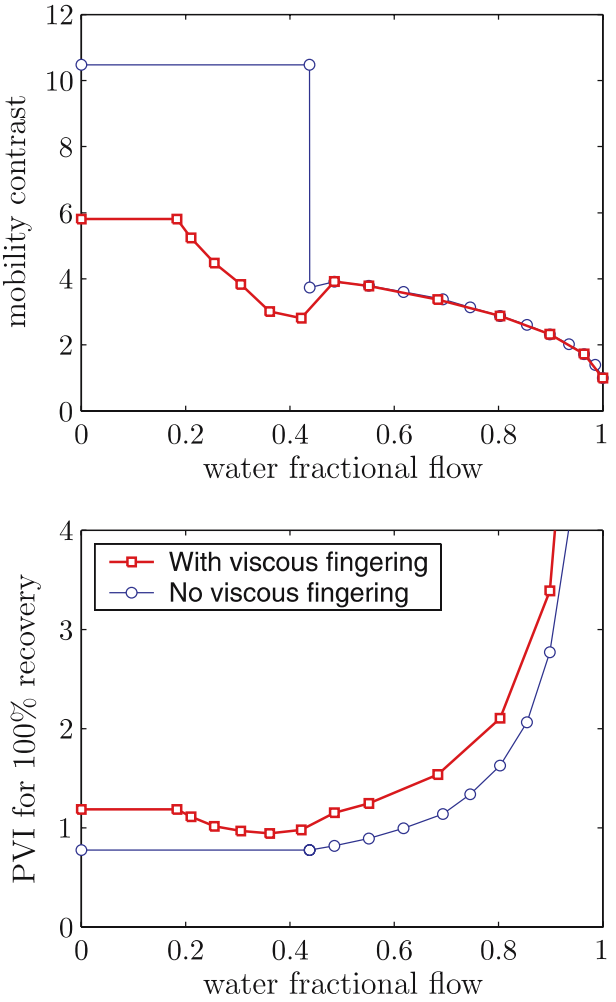

Figure 23. Dependence of the mobility ratio across the solvent front and the number of PVI for 100% recovery. The predictions using a self-consistent M_{eff} are compared with those when viscous fingering is ignored.

WAG ratio is then taken as a value slightly above the critical value, $W_R^{\text{opt}} \approx 0.78$, because it combines the highest displacement efficiency $\text{PVI}^{\text{opt}} \approx 0.77$ with a relatively low value of the mobility contrast.

The model *with* viscous fingering, on the other hand, predicts a continuous dependence of the displacement efficiency and the *self-consistent* mobility ratio across the solvent front with respect to the water–solvent ratio. The curves of PVI and mobility ratio both show a minimum at approximately the same water fractional flow. The minimum of the PVI curve corresponds to $W_R^{\text{opt}} \approx 0.56$, for which $\text{PVI}^{\text{opt}} \approx 0.94$.

The differences between the two models are exactly what one would expect. Because the solvent fingers through, the displacement is less efficient than what the fingering-free model predicts. Thus, more solvent is required at the optimum WAG ratio (38% difference), and more pore volumes need to be injected to recover all the oil (22% difference).

6. Conclusions and Future Work

In this paper, we have revisited an empirical model of three-component, two-phase, first-contact miscible flow that includes the effects of viscous fingering. The model was originally presented in Blunt and Christie (1993, 1994), where analytical solutions were developed for secondary and tertiary WAG floods, and validated by comparison with the average profiles of highly detailed multidimensional simulations. Here, we have analyzed the mathematical character of the system of equations in detail, showing that the system is strictly hyperbolic almost everywhere, except for the region of residual hydrocarbon saturations and two states on the edges of the ternary diagram, where the system displays a parabolic degeneracy. Our analysis also includes the evaluation of the integral curves (composition paths) in phase space, and the location of the inflection loci of each of the characteristic fields. We have presented the complete range of analytical solutions to secondary and tertiary WAG floods. An important element of our analysis is a study of the Hugoniot locus of the initial states. We have shown that detached branches of the Hugoniot locus are essential in the construction of the solution for tertiary floods. We have illustrated how, in WAG tertiary floods, the solvent front and the water Buckley-Leverett front may interact. The result of that interaction is a leading shock that involves changes in *both* water saturation and solvent mass fraction, and is stable to viscous fingering. The main features of the solution persist even when the dispersive effects of viscous fingering are limited by the use of a self-consistent effective mobility ratio. The analytical solutions explain why, in miscible tertiary floods, oil and solvent may break through simultaneously. We have also shown that accounting for viscous fingering affects the predictions of the optimum WAG ratio for tertiary floods, and that the proportion of injected solvent should be higher than that obtained with Stalkup's method.

An important consideration is whether the mathematical model presented here is successful at reproducing experimental observations. For instance, the one-dimensional model makes use of a multiphase extension of the Todd and Longstaff model developed for single-phase flow. It is not obvious that this model yields accurate predictions when the saturation of the second phase (water) changes along the oil–solvent mixing zone. Also, the analytical model predicts that the leading edge of the oil bank

is stable with respect to viscous fingering, but it is unclear whether pressure oscillations associated with viscous fingering in a multidimensional setting may induce instabilities. We have recently addressed these issues and *validated* the model, in particular, for situations in which oil and solvent break through simultaneously. Validation of the model was accomplished by means of high-resolution direct numerical simulations that resolve the details of viscous fingering and carefully designed laboratory experiments (Juanes *et al.*, submitted). The conclusion of that investigation is that the parameter-free, one-dimensional analytical model yields accurate quantitative predictions of the macroscopic effects of viscous fingering in two-phase, three-component flow.

The work presented here is the first step towards the development of a complete Riemann solver for this problem, that is, an algorithm that computes the exact solution for *any* initial and injected states. The Riemann solver should account for the dynamic calibration of the effective mobility ratio M_{eff}, which introduces additional complexity because the composition paths depend on the value of M_{eff}. Such Riemann solver could then be used as a building block in a front-tracking algorithm to compute approximate solutions to the transport equations along streamlines, leading to accurate and efficient simulation of multiphase first-contact miscible flow in three-dimensional heterogeneous formations (Juanes and Lie, 2005; Lie and Juanes, 2005).

Acknowledgements

R.J. gratefully acknowledges financial support from the industrial affiliates of the Stanford University Petroleum Research Institute for Numerical Simulation (SUPRI-B) and Gas Injection (SUPRI-C). We thank the Reviewers for their insightful comments, which led to a substantial improvement of the paper.

References

Ancona, F. and Marson, A.: 2001, A note on the Riemann problem for general $n \times n$ conservation laws, *J. Math. Anal. Appl.* **260**, 279–293.

Barkve, T.: 1989, The Riemann problem for a nonstrictly hyperbolic system modeling nonisothermal two-phase flow in a porous medium, *SIAM J. Appl. Math.* **49**(3), 784–798.

Blackwell, R. J., Rayne, J. R. and Terry, W. M.: 1959, Factors influencing the efficiency of miscible displacements, *Petrol. Trans. AIME* **216**, 1–8.

Blunt, M. and Christie, M.: 1993, How to predict viscous fingering in three component flow, *Transp. Porous Media* **12**, 207–236.

Blunt, M. and Christie, M.: 1994, Theory of viscous fingering in two phase, three component flow, *SPE Adv. Technol. Ser.* **2**(2), 52–60.

Blunt, M. J., Barker, J. W., Rubin, B., Mansfield, M., Culverwell, I. D. and Christie, M. A.: 1994, Predictive theory for viscous fingering in compositional displacement, *SPE Reserv. Eng.* **9**(1), 73–80.

Caudle, B. H. and Dyes, A. B.: 1958, Improving miscible displacement by gas–water injection, *J. Pet. Technol. Petrol. Trans. AIME* **213**, 281–284.

Chang, Y.-B., Lim, M. T., Pope, G. A. and Sepehrnoori, K.: 1994, CO_2 flow patterns under multiphase flow: heterogeneous field-scale conditions, *SPE Reserv. Eng.* **9**(3), 208–216.

Chen, C. Y. and Meiburg, E.: 1998, Miscible porous media displacements in the quarter five-spot configuration. Part 1. The homogeneous case, *J. Fluid Mech.* **371**, 233–268.

Christie, M. A.: 1989, High-resolution simulation of unstable flows in porous media, *SPE Reserv. Eng.* **4**, 297–303.

Christie, M. A. and Jones, A. D. W.: 1987, Comparison between laboratory experiments and detailed simulation of miscible viscous fingering, in: *Fourth European Symposium on Enhanced Oil Recovery*, Hamburg, Germany.

Christie, M. A., Jones, A. D. W. and Muggeridge, A. H.: 1990, Comparison between laboratory experiments and detailed simulations of unstable miscible displacement influenced by gravity, in: A. T. Buller *et al.* (eds), *North Sea Oil and Gas Reservoirs–II: Proceedings of the Second North Sea Oil and Gas Reservoirs Conference (Trondheim, Norway, 8–11 May, 1989)*, Graham & Trotman, Norwell, MA, pp. 245–250.

Christie, M. A., Muggeridge, A. H. and Barley, J. J.: 1993, 3D simulation of viscous fingering and WAG schemes, *SPE Reserv. Eng.* **8**, 19–26.

da Mota, J. C.: 1992, The Riemann problem for a simple thermal model for two phase flow in porous media, *Mat. Aplic. Comp.* **11**(2), 117–145.

de Souza, A. J.: 1992, Stability of singular fundamental solutions under perturbations for flow in porous media, *Mat. Aplic. Comp.* **11**(2), 73–115.

Falls, A. H. and Schulte, W. M.: 1992, Features of three component, three phase displacement in porous media, *SPE Reserv. Eng.* **7**(4), 426–432.

Fayers, F. J., Blunt, M. J. and Christie, M. A.: 1992, Comparison of empirical viscous-fingering models and their calibration for heterogeneous problems, *SPE Reserv. Eng.* **7**, 195–203.

Helfferich, F. G.: 1981, Theory of multicomponent, multiphase displacement in porous media, *Soc. Pet. Eng. J.* **21**(1), 51–62. *Petrol. Trans. AIME* **271**.

Homsy, G. M.: 1987, Viscous fingering in porous media, *Ann. Rev. Fluid Mech.* **19**, 271–311.

Isaacson, E., Marchesin, D., Plohr, B. and Temple, J. B.: 1992, Multiphase flow models with singular Riemann problems, *Mat. Aplic. Comp.* **11**(2), 147–166.

Johansen, T. and Winther, R.: 1988, The solution of the Riemann problem for a hyperbolic system of conservation laws modeling polymer flooding, *SIAM J. Math. Anal.* **19**(3), 541–566.

Juanes, R.: 2005, Determination of the wave structure of the three-phase flow Riemann problem, *Transp. Porous Media* **60**(2), 135–139.

Juanes, R., Al-Shuraiqi, H. S., Muggeridge, A. H., Grattoni, C. A. and Blunt, M. J.: 2005, Experimental and numerical validation of an analytical model of viscous fingering in two-phase, three-component flow, *J Fluid Mech.* (Submitted).

Juanes, R. and Lie, K.-A.: 2005, A front-tracking method for efficient simulation of miscible gas injection processes, in: *SPE Reservoir Simulation Symposium*, Houston, TX, January 31-February 2 2005. (SPE 93298).

Juanes, R. and Patzek, T. W.: 2004, Analytical solution to the Riemann problem of three-phase flow in porous media, *Transp. Porous Media* **55**(1), 47–70.

Khan, S. A., Pope, G. A. and Trangenstein, J. A.: 1996, Micellar/Polymer physical-property models for contaminant cleanup problems and enhanced oil recovery, *Transp. Porous Media* **24**(1), 35–79.

Koval, E. J.: 1963, A method for predicting the performance of unstable miscible displacements in heterogeneous media, *Soc. Pet. Eng. J. Petrol. Trans. AIME* **219**, 145–150.

Lake, L. W.: 1989, *Enhanced Oil Recovery*, Prentice-Hall, Englewood Cliffs, NJ.
Lax, P. D.: 1957, Hyperbolic systems of conservation laws, II, *Comm. Pure Appl. Math.* **10**, 537–566.
Lenormand, R., Touboul, E. and Zarcone, C.: 1988, Numerical models and experiments on immiscible displacements in porous media, *J. Fluid Mech.* **189**, 165–187.
Lie, K.-A. and Juanes, R.: 2005, A front-tracking method for the simulation of three-phase flow in porous media, *Comput. Geosci.* 9(1), 29–59
Lin, E. C. and Huang, E. T. S.: 1990, The effect of rock wettability on water blocking during miscible displacement, *SPE Reserv. Eng.* **5**(2), 205–212.
Liu, T.-P.: 1974, The Riemann problem for general 2×2 conservation laws, *Trans. Amer. Math. Soc.* **199**, 89–112.
Marchesin, D. and Plohr, B. J.: 2001, Wave structure in WAG recovery, *Soc. Petrol. Eng. J.* **6**(2), 209–219.
Muskat, M.: 1949, *Physical Principles of Oil Production*, McGraw-Hill, New York.
O'Steen, B. L. and Huang, E. T. S.: 1990, Modeling of trapped and dendritic oil mobilization during miscible displacement, *In Situ* **14**(3), 285–343.
Pope, G. A.: 1980, The application of fractional flow theory to enhanced oil recovery, *Soc. Pet. Eng. J.* **20**(3), 191–205, *Petrol. Trans. AIME* **269**.
Ruith, M. and Meiburg, E.: 2000, Miscible rectilinear displacements with gravity override. Part 1. Homogeneous porous medium, *J. Fluid Mech.* **420**, 225–257.
Saffman, P. G. and Taylor, G. I.: 1958, The penetration of a fluid into a porous medium or Hele–Shaw cell containing a more viscous liquid, *Proc. R. Soc. London Ser. A* **245**, 312–329.
Schaeffer, D. G. and Shearer, M.: 1987a, Riemann problems for nonstrictly hyperbolic 2×2 systems of conservation laws, *Trans. Amer. Math. Soc.* **304**(1), 265–306.
Schaeffer, D. G. and Shearer, M.: 1987b, The classification of 2×2 systems of nonstrictly hyperbolic conservation laws, with application to oil recovery, *Comm. Pure Appl. Math.* **40**(1), 141–178. Appendix with D. Marchesin and P. J. Paes-Leme.
Schecter, S., Marchesin, D. and Plohr, B. J.: 1996, Structurally stable Riemann solutions, *J. Differ. Equations* **126**, 303–354.
Smoller, J.: 1994, *Shock Waves and Reaction-Diffusion Equations*, 2nd edn, Springer-Verlag, New York.
Spiteri, E. J. and Juanes, R.: 2006, Impact of relative permeability hysteresis on the numerical simulation of WAG injection, *J. Petrol. Eng. Sci.* (in press).
Spiteri, E. J., Juanes, R., Blunt, M. J. and Orr, Jr., F. M.: 2005, Relative permeability hysteresis: trapping models and application to geological CO_2 sequestration, in: *SPE Annual Technical Conference and Exhibition*, Dallas, TX, October 9–12 2005. (SPE 96448)
Stalkup, Jr, F. I.: 1983, *Miscible Displacement*, Society of Petroleum Engineers, Dallas, TX.
Tan, C. T. and Homsy, G. M.: 1988, Simulation of nonlinear viscous fingering in miscible displacement, *Phys. Fluids* **6**, 1330–1338.
Tchelepi, H. A. and Orr, F. M.: 1994, Interaction of viscous fingering, permeability heterogeneity and gravity segregation in three dimensions, *SPE Reserv. Eng.* **9**(4), 266–271.
Todd, M. R. and Longstaff, W. J. 1972, The development, testing and application of a numerical simulator for predicting miscible flood performance, *J. Petrol. Technol.* 874–882.
Walsh, M. P. and Lake, L. W.: 1989, Applying fractional flow theory to solvent flooding and chase fluids, *J. Petrol. Sci. Eng.* **2**, 281–303.
Zauderer, E.: 1983, *Partial Differential Equations of Applied Mathematics,* John Wiley & Sons, New York.
Zimmerman, W. B. and Homsy, G. M.: 1991, Nonlinear viscous fingering in miscible displacement with anisotropic dispersion, *Phys. Fluids A* **8**(3), 1859–1872.